
BUFFER REPLAY ENHANCES THE ROBUSTNESS OF MULTIMODAL LEARNING UNDER MISSING-MODALITY *

Zhu Hongye, Xuan Liu, Yanwen Ba, Jingye Xue
College of Computer Science and Electronic Engineering
Hunan University
Changsha, China
{Zhuhongye, XuanLiu, YanwenBa, JingyeXue}@hnu.edu.cn

Shigeng Zhang
School of Computer Science
Central South University
Changsha, China
sgzhang@csu.edu.cn

ABSTRACT

Missing modalities consistently lead to significant performance degradation in multimodal models. Existing approaches either synthesize missing modalities at high computational cost or apply prompt-based fine-tuning that relies only on adjacent-layer features and overlooks long-distance contextual information. Such information may offer additional tolerance to errors in scenarios where one or more modalities are missing. Therefore, REplay Prompting (REP) is introduced. Specifically: (1) modality-wise feature buffers are constructed via a residual bypass to cache early-layer representations and replay them in deeper layers, mitigating information loss as network depth increases; (2) a private-shared feature decoupling strategy is employed, where private buffers preserve fine-grained modality-specific signals while shared buffers encode cross-modal semantics; and (3) a task-aware dynamic initialization mechanism is designed to configure these buffers differently, improving stability and generalization under diverse missing-modality conditions. Experiments on vision-language, vision-language-audio, and temporal multimodal benchmarks show that REP consistently surpasses prior methods under both single- and multi-modality missing conditions, while adding only negligible parameter overhead. These results position REP as a lightweight yet highly effective paradigm for robust multimodal learning in challenging missing-modality scenarios. Code is available at <https://github.com/ZhyHNU/REP>.

Keywords Missing modality · Prompt fine-tuning · Multimodal-Learning

1 Introduction

The rapid development of multimodal learning has given rise to powerful Transformer models, including vision-language models (e.g., [1]) and audio-text models (e.g., [2]). These models can effectively leverage information across different modalities and demonstrate excellent performance in tasks such as sentiment analysis [3, 4], visual recognition [5, 6, 7], and cross-modal retrieval [5]. However, missing modalities are common in real-world applications due to factors like sensor malfunctions, privacy constraints, or harsh environments, often making certain modalities unavailable.

This lack of modality is a significant challenge, as it severely degrades model performance and is a major barrier to the real-world deployment of multimodal technologies. In standard multimodal tasks, redundant information across modalities provides a fault-tolerant buffer. For example, blurry visual features can be compensated by clear textual descriptions. However, in missing-modality scenarios, models often cannot access enough redundant information to fill the gap. As illustrated in Figure 1(a), when the text modality is missing, the model may incorrectly identify the category, significantly affecting its recognition ability and performance [8, 9].

Modality completion methods rely on generative models to reconstruct missing modalities. Although these approaches have shown progress, they often introduce noise and artificial semantic artifacts during generation, while also incurring considerable computational overhead during both training and inference [10, 11]. In contrast, prompt-based fine-tuning provides a more efficient paradigm. For example, MAP and DCP [12, 13] treat missing modalities as prompt inputs and

**Citation: Authors. Title. Pages.... DOI:000000/11111.*

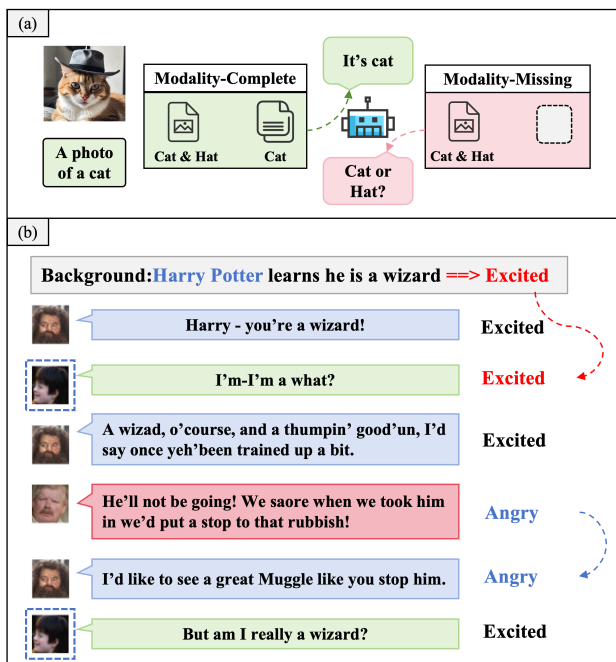


Figure 1: Motivation of the proposed work (a) Modality missing may impair the model’s understanding of the task and its ability to correctly recognize categories. (b) Long-distance contextual information is crucial for multimodal emotion recognition; local modeling errors may introduce bias into the global prediction.

fine-tune the model using mechanisms such as attention prompts or deep-correlation prompts, enabling the model to handle different missing-modality conditions more effectively during inference. However, these methods primarily rely on updates from adjacent-layer features, overlooking the degradation of modality-specific information in early layers. As illustrated in Figure 1(b), many tasks—such as emotion recognition—depend heavily on long-range contextual information across layers, and partial modality absence can substantially impair global understanding. Furthermore, the compensatory roles of private and shared features under different missing-modality scenarios remain insufficiently modeled.

This paper introduces *Replay Prompting (REP)* for missing modality scenarios. First, we propose a feature caching and replay mechanism. Traditional methods update prompts using only adjacent-layer features. In contrast, our approach preserves early-layer representations through residual bypass feature buffers. By replaying feature buffers into the deeper layers, it effectively alleviates the information decay that occurs with increasing network depth, thereby providing potential information compensation for missing modalities. Then, we introduce a private-shared feature decoupling strategy. REP adopts a dual-buffer, the private buffer stores modality-specific details, while the shared buffer captures cross-modal information. These buffers are separated using orthogonality constraints and are updated independently. Moreover, to further enhance generalization, we introduce a task-aware dynamic initialization that dynamically initializes the buffers based on the task type and input sample, improving generalization and robustness. REP achieves significant performance improvements across several multimodal benchmarks (covering mainstream modalities such as vision, language, audio, and temporal data) with only a 0.2% increase in fine-tuning parameters. It consistently achieves state-of-the-art (SOTA) performance in both single-modality and multimodal missing settings, while maintaining an excellent balance between lightweight efficiency and robust high performance.

Overall, the main contributions of this paper include:

- Using caching and replay mechanisms to mitigate information decay, providing a fault-tolerant buffer and improving the model’s robustness in scenarios with missing modalities.
- Explicitly modeling private and shared features, capturing modality-specific private information and shared cross-modal information, respectively.
- The dynamic buffer strategy enhances robustness and generalization.

2 Related work

Prompt learning adapts pre-trained models to downstream tasks by introducing learnable prompt tokens into the input space, enabling efficient fine-tuning with minimal parameter updates. Visual Prompt Tuning [14] embeds learnable visual prompts into images, while CLIP [1] employs hand-crafted text templates to align images and text for strong few-shot performance. CoOp [15] replaces manual templates with learnable text prompts, and CoCoOp [16] generates prompts conditioned on image features to improve generalization to unseen classes. Progressive Prompts [17] further compose task-specific prompts progressively during training, allowing the prompt complexity to adapt over time.

Missing modality in multimodal learning was first introduced and benchmarked by (author?) [18]. MAP [12] treats different missing modalities as independent inputs, but its prompts are initialized with zero matrices, lacking correlation with the inputs. DCP [13] extends this idea by generating dynamic prompts based on the correlation between input features and prompts; however, its Gaussian-based random generation limits adaptability across diverse scenarios. For multimodal sentiment analysis where image, text, or audio modalities may be missing, (author?) [11] introduces generative, missing-signal, and missing-type prompts to handle various missing cases, while [19] explores fine-tuning Transformers on small-scale data under the read-only prompt framework [20] to preserve generalization and stability. MaPLe [21] and DePT [22] further enhance cross-task transferability by coupling visual–language prompts and disentangling task-specific from shared knowledge, respectively. LNLN[23] treats language as the dominant modality and enhances sentiment recognition robustness across various random missing and noise scenarios through dominant-modality correction. In addition, [24, 25, 26] conducted in-depth studies on the problem of incomplete modalities in recommendation systems and multimodal sentiment analysis.

Above methods have been mainly validated on vision-language or limited multimodal tasks with specific modality combinations. In contrast, we extend our approach to broader multimodal scenarios involving images, text, audio, and sensor signals. Since existing prompt designs rarely address long-distance modeling under missing modalities, we introduce a replay-based mechanism to better capture long-term and historical dependencies. We also systematically investigate how different prompt initialization strategies influence model robustness.

3 Methods

3.1 Overview

This section introduces REP, a novel multimodal robustness framework designed specifically for modality-missing scenarios. As illustrated in the workflow of Figure 2, section 3.2 first presents the definition of modality-missing settings. Following this, section 3.3 introduces the private–shared feature decoupling strategy and explains how the two buffers are cached and updated. Section 3.4 then demonstrates how feature replay is performed at the current layer. Finally, we show the task-aware dynamic initialization strategy in 3.5, detailing how the two buffers are initialized differently and how this design ultimately enhances generalization.

3.2 Problem Definition

We consider a multimodal learning task involving K modalities, whose modality set is defined as:

$$\mathcal{M} = \{m_1, m_2, \dots, m_K\}. \quad (1)$$

For each task, the multimodal representation is formulated as:

$$T = \{x^{m_1}, x^{m_2}, \dots, x^{m_K}, y, \eta\}, \quad (2)$$

where x^{m_i} denotes the input feature of modality m_i , y is the corresponding label, and η is the modality missing rate.

We denote the set of missing modalities as $\mathcal{M}_{\text{miss}} \subseteq \mathcal{M}$, and use the modality missing rate $\eta \in [0, 1]$ to indicate the proportion of missing information. To distinguish different missing cases, we further define:

- **Single-modality missing rate** η_s : the proportion of missing information when only one modality is missing;
- **Multi-modality missing rate** η_m : the total proportion of missing information when multiple modalities are simultaneously missing.

In a vision-language task, if the visual modality is missing with a missing rate of $\eta_s = 70\%$, the sample is represented as:

$$T^{\mathcal{M}_{\text{miss}}(v)} = \{\tilde{x}^{m_1}, x^{m_2}, y, \eta_s = 70\%\}, \quad (3)$$

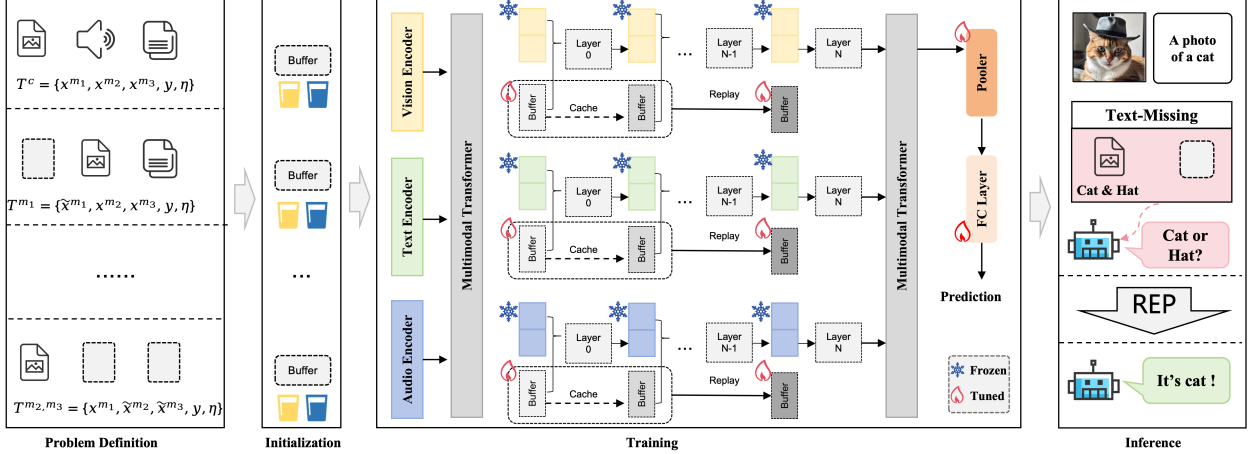


Figure 2: Workflow of the proposed REP. (1) Missing scenarios are defined, and different missing types are initialized into private or shared buffers. (2) These buffers cache information from the first $k - 1$ layers via residual bypass during fine-tuning, and the cached information is replayed in the $k - th$ layer. (3) During inference, the REP fine-tuned model significantly improves recognition accuracy under missing modality conditions.

where \tilde{x}^{m_1} denotes the placeholder input for the missing visual modality.

For example, if both visual and textual modalities are missing, the sample is defined as:

$$T^{\mathcal{M}_{\text{miss}}(v,l)} = \{\tilde{x}^{m_1}, \tilde{x}^{m_2}, y, \eta_m = 100\%\}, \quad (4)$$

where $\eta_m = 100\%$ indicates that the total missing proportion of both modalities is 100%, thus the missing rate for each modality is $\frac{\eta_m}{|\mathcal{M}_{\text{miss}}|} = 50\%$.

3.3 Private-shared feature decoupling

Existing multimodal models typically rely on cross-modal shared features for inference tasks. However, when a single modality is missing, modality-specific information may provide potential compensation. Therefore, as shown in Figure 3, we designed a dual-buffer structure to separately capture modality-specific information and cross-modal common semantics.

3.3.1 Feature Separation

The private and shared buffers are maintained through independent initialization and update paths, ensuring effective separation of the two feature types. At layer 0, these two kinds of features, together with the original input embeddings, appear in the following form:

$$\tilde{\mathbf{E}}_m[0] = [\Theta_m(\mathbf{F}_s), \mathbf{F}_p^m[0], \mathbf{E}_m[0]] \quad (5)$$

Here, $\Theta_m(\mathbf{F}_s)$ is the shared feature projected into the modality m space, $\mathbf{F}_p^m[0]$ is the modality m private feature, and $\mathbf{E}_m[0]$ is the original input embedding. The three parts are concatenated along the sequence length dimension and input to the Transformer.

To ensure the independence of shared and private features, an orthogonality constraint loss is imposed:

$$\mathcal{L}_{\text{ortho}} = \sum_{k=1}^K \left(\langle \mathbf{F}_s, \mathbf{F}_p^m[k] \rangle + \sum_{m \neq m'} \langle \mathbf{F}_p^m[k], \mathbf{F}_p^{m'}[k] \rangle \right) \quad (6)$$

where $\langle \cdot, \cdot \rangle$ denotes the inner product operation, which measures the similarity between feature vectors. The first term enforces orthogonality between shared and private features, while the second term ensures the orthogonality of private features across different modalities. By minimizing these inner product values, this constraint ensures that the shared

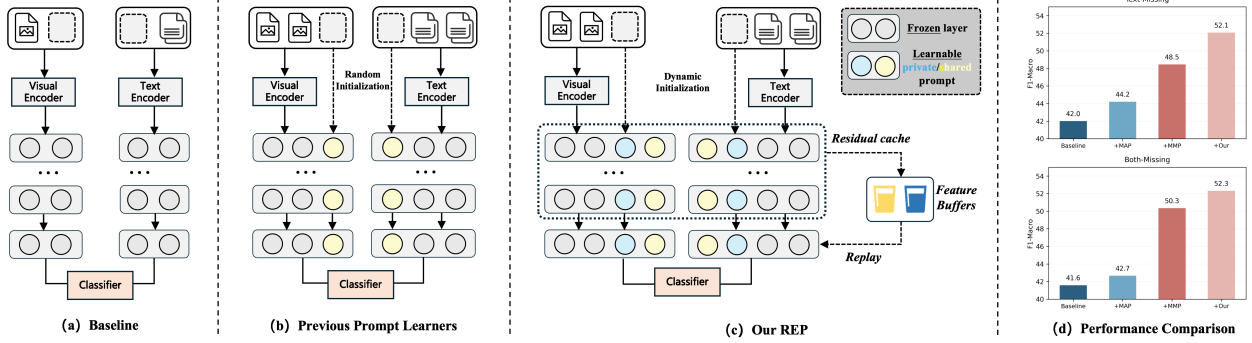


Figure 3: (a) Baseline is the CLIP model, using ViT-B/16 as the visual encoder. (b) Previous works such as MAP, MMP, and DCP use random or zero initialization, treating different missing scenarios as independent inputs and fine-tuning the model with prompts. (c) Our proposed REP adopts task-dependent dynamic initialization, caching feature buffers through residual bypass, storing shared and private features separately, and replaying them in deeper layers. (d) Comparison on MM-IMDb, where the missing rate for text-missing is 70%, and for both-missing, each modality is missing 35% (total missing rate is also 70%).

space captures cross-modal consistency, while the private space retains modality-specific uniqueness. This constraint is added as a regularization term to the CLIP loss.

3.3.2 Private Buffer Update

The private buffer \mathbf{F}_p^m stores modality-specific features that reflect unique characteristics of each modality (e.g., visual textures, semantic patterns, or acoustic cues). At each layer k , the private buffer is updated through the residual bypass mechanism, which adapts to new features while preserving historical memory:

$$\mathbf{F}_p^m[k] = \alpha_m \cdot G_m(\mathbf{Z}_p^m[k]) + (1 - \alpha_m) \cdot \mathbf{F}_p^m[k - 1] \quad (7)$$

Here, $\mathbf{Z}_p^m[k]$ represents the current features extracted at layer k for modality m , processed through normalization and a lightweight transformation network $G_m(\cdot)$ (composed of two layers of MLP and GELU). The coefficient α_m is a learnable scalar that controls the balance between current features and historical memory. A higher α_m places more emphasis on the current layer’s features, while a lower value emphasizes accumulated historical information. This update mechanism, in the form of residual and bypass storage, preserves low-level details while dynamically integrating new layer semantics, allowing the buffer to continuously accumulate and consolidate modality-specific information.

3.3.3 Shared Buffer Update

The shared buffer \mathbf{F}_s stores cross-modal common semantic information. Similar to the private buffer, the shared buffer is also updated through the residual bypass mechanism to maintain semantic consistency and provide compensation in the case of missing modalities:

$$\mathbf{F}_s[k] = \varepsilon_s \cdot H(C(\{\mathbf{F}_p^m[k]\}_m)) + (1 - \varepsilon_s) \cdot \mathbf{F}_s[k - 1] \quad (8)$$

Here, $C(\cdot)$ represents the concatenation of the private buffer features from all modalities. $H(\cdot)$ is the shared feature update network (a single-layer MLP with GELU activation) that maps the concatenated features to the shared semantic space. The coefficient ε_s controls the update rate of the shared features.

3.4 Feature Replay

Before entering each Transformer layer, the model performs feature replay by concatenating the private and shared buffer features from earlier layers with the current input features. This process enhances the representation by injecting historical memory into the current layer:

$$\tilde{\mathbf{E}}_m[k] = \mathbf{E}_m[k] + \beta_p \cdot \mathbf{F}_p^m[k - 1] + \beta_s \cdot \mathbf{F}_s[k - 1] \quad (9)$$

Here, $\mathbf{E}_m[k]$ represents the input embedding of modality m at layer k , while $\mathbf{F}_p^m[k-1]$ and $\mathbf{F}_s[k-1]$ are the private and shared memory features from the previous layer. The weights β_p and β_s control the amount of historical information injected into the current input. This layer-wise replay mechanism allows the model to access both immediate input and historical memory, creating a hierarchical flow of information from shallow to deep layers. The residual bypass replay mechanism strengthens the model’s cross-modal reasoning ability and robustness to missing modalities, enabling it to leverage complete historical context. The aforementioned factors α_m , ε_s and β are adjusted adaptively and require no manual tuning.

It is important to note that the depth d of the buffers is determined by the number of layers k , while the initial feature embedding length l determines the width of the buffers. These two factors together define the buffer size and the associated parameters and computational costs. In our experiments, we explore the relationship between buffer depth d , width l , and performance, aiming to maximize performance while minimizing parameter growth.

3.5 Dynamic Initialization

In the REP method, dynamic initialization initializes feature memory buffers by adding controlled noise to pre-trained modality features, ensuring each modality retains its unique information while introducing sufficient diversity and robustness.

For each modality m , the private buffer’s initial features are obtained by adding perturbations to the pre-trained embeddings:

$$\mathbf{F}_{\text{private}}^m[0] = \mathcal{E}_m + \epsilon_n \zeta_m, \quad \zeta_m \sim \mathcal{N}(0, \mathbf{I}) \quad (10)$$

where $\mathbf{F}_{\text{private}}^m[0]$ denotes the initial features of the private buffer for modality m , with \mathcal{E}_m as the pre-trained embedding, and ϵ_n controlling the noise intensity. ζ_m is noise sampled from a standard normal distribution, with independent samples across modalities. This process introduces controlled diversity to each modality’s initial representation, improving generalization.

The shared buffer is initialized with normalized Gaussian noise to provide a flexible semantic space for cross-modal collaboration:

$$\mathbf{F}_{\text{shared}}[0] = \frac{\boldsymbol{\xi}}{\|\boldsymbol{\xi}\|_2}, \quad \boldsymbol{\xi} \sim \mathcal{N}(0, \mathbf{I}) \quad (11)$$

where $\mathbf{F}_{\text{shared}}[0]$ stores cross-modal common semantic information. $\boldsymbol{\xi}$ is a random vector sampled from the standard normal distribution, with the normalization ensuring the vector lies on the unit hypersphere. This initialization strategy enables flexible cross-modal collaboration while avoiding numerical instability.

This dynamic initialization strategy ensures diversified initial features for each modality while maintaining separation between shared and private information. In the experiments, we analyze the impact of ϵ_n and different noise types on performance.

4 Experiments

4.1 Implementation Details

4.1.1 Benchmark

We construct a systematic benchmark covering two multimodal task settings: vision-language (VL), vision-language-audio (VLA) and acoustic-seismic (AS).

VL Benchmark includes three datasets: MM-IMDb (F1-Macro) [28], UPMC Food-101 (accuracy)[29], and Hateful Memes (AUROC) [30]. These datasets span multimodal sentiment analysis, food image-text recognition, and cross-modal sarcasm detection. The baseline model is CLIP [1], where the image encoder is ViT-B/16, and we directly use publicly released pre-trained weights.

VLA Benchmark is conducted on CH-SIMS [31] and MOSI [32], using ACC and F1 as evaluation metrics. These datasets cover vision-text-audio multimodal sentiment analysis. The baseline model is MuLT [33], pre-trained on the CMU-MOSEI dataset [34] without prompts.

Table 1: Comparison of performance on MM-IMDb, Food101, and Hateful Memes datasets under different missing modality rates η . Bold values indicate the best performance.

Dataset	Missing rate η	Train / Test		Methods							
		Image	Text	Baseline	CoOp [15]	MAP [12]	MaPLe [21]	DePT [22]	MMP [27]	DCP [13]	Ours
MM-IMDb (F1-Macro)	50%	100%	50%	44.73	48.06	48.88	49.58	50.64	49.21	52.13	54.05
		50%	100%	45.96	49.89	51.46	52.32	52.78	53.67	54.32	55.40
		75%	75%	44.12	48.37	49.32	49.56	50.87	51.09	52.46	55.27
	70%	100%	30%	42.02	44.13	44.22	45.52	46.38	48.46	48.52	52.08
		30%	100%	42.95	46.88	46.30	50.64	52.13	52.62	53.14	53.71
		65%	65%	41.64	46.84	42.66	48.30	50.32	50.34	51.69	52.31
	90%	100%	10%	40.31	44.06	45.32	46.84	47.56	42.07	49.26	50.05
		10%	100%	46.02	49.89	50.13	50.88	51.22	51.23	51.95	52.05
		55%	55%	40.18	44.12	44.87	45.12	46.54	47.81	48.44	50.76
Food101 (Accuracy)	50%	100%	50%	72.18	77.45	77.89	79.64	80.16	78.81	82.11	83.65
		50%	100%	80.16	87.02	87.16	87.35	82.14	86.90	88.29	88.56
		75%	75%	75.49	81.82	81.72	82.34	83.12	82.35	85.24	85.55
	70%	100%	30%	70.42	76.34	74.53	77.02	77.34	75.41	78.87	80.40
		30%	100%	78.11	84.78	86.18	85.89	86.12	87.11	87.32	87.22
		65%	65%	73.02	78.87	79.08	79.84	81.46	81.22	81.87	82.68
	90%	100%	10%	66.41	71.87	73.14	73.46	74.12	78.13	75.26	77.86
		10%	100%	76.68	83.12	83.96	83.12	83.56	84.35	85.78	88.54
		55%	55%	70.31	76.46	76.58	77.85	78.12	79.67	79.87	80.33
Hateful Memes (AUROC)	50%	100%	50%	55.77	60.56	60.31	60.87	61.87	62.12	62.32	69.92
		50%	100%	57.62	62.41	62.35	63.13	63.88	64.01	64.46	66.23
		75%	75%	59.83	64.87	65.84	65.46	65.86	65.42	66.02	67.44
	70%	100%	30%	57.44	62.60	59.11	63.14	63.84	61.39	64.12	70.01
		30%	100%	58.71	64.07	63.06	64.12	64.54	65.24	65.48	66.17
		65%	65%	59.54	64.82	66.07	65.23	65.48	65.17	66.08	66.89
	90%	100%	10%	55.29	60.03	57.21	60.71	61.14	62.06	62.08	68.92
		10%	100%	56.92	61.46	61.52	61.87	62.42	61.97	63.57	63.87
		55%	55%	57.41	62.93	63.34	63.68	63.12	64.27	64.58	64.77

AS Benchmark is evaluated on the MOD dataset[35], which is used for mobile objects (vehicle, human) classification. And model is pre-trained on the MOD pre-training dataset.

4.1.2 Missing Settings

We use fixed placeholder inputs to simulate unavailable modalities while maintaining consistent input structure:

- **Text-missing:** Empty string \rightarrow minimal valid text embedding via tokenizer
- **Image-missing:** All-one pixel image \rightarrow semantics-free visual representation via patch embedding
- **Audio-missing:** Fixed-length all-zero vector \rightarrow minimal semantic audio embedding via front-end encoder

4.2 Results on VL tasks

To validate the robustness and generalization capabilities of our proposed method, we introduce different modality missing rates and various missing scenarios across three VL datasets. For example, missing rate $\eta = 70\%$ corresponds to severe missing conditions, including image-only missing 70%, text-only missing 70%, or both modalities missing 35% each. The comparison results are shown in Table 1, with the best results highlighted in bold.

REP demonstrates consistent performance advantages across all 27 experimental configurations. Its superiority is particularly evident on the Hateful Memes dataset, where it achieves the best results in all nine missing-modality settings, outperforming the second-best method DCP by an average of 4.5 percentage points. Under severe missing conditions ($\eta = 70\%$), REP attains 52.08 F1-Macro on MM-IMDb and 70.01 AUROC on Hateful Memes, corresponding to improvements of 7.3% and 9.2%, respectively. In extreme missing scenarios ($\eta = 90\%$), where either the text or image modality is nearly absent, the advantage of REP becomes even more pronounced. For example, under the text-severely-missing condition on Hateful Memes, REP surpasses DCP by 11%, indicating that the cross-layer feature buffering and replay mechanism effectively leverages historical information from complete modalities to compensate for missing signals, thereby providing greater fault tolerance and significantly improving prediction stability. Overall,

Table 2: Comparison on **CH-SIMS**, **MOSEI**, and **MOSI** datasets under missing rate $\eta = 70\%$. [Audio-only] indicates that the other two modalities are missing, each with a missing rate of 35%. [Audio-Missing] indicates that only the audio modality is missing, with a missing rate of 70%. Bold values indicate the best performance.

Dataset	Method	Audio-only		Image-only		Text-only		Text-missing		Image-missing		Audio-missing		Avg.	
		Acc	F1	Acc	F1	Acc	F1	Acc	F1	Acc	F1	Acc	F1	Acc	F1
CH-SIMS	MMIN	65.21	77.09	64.28	73.36	78.91	78.67	77.32	77.33	77.40	77.48	77.40	77.48	73.42	76.90
	LNLN	64.98	76.41	64.01	73.47	78.56	78.65	77.11	77.20	77.51	77.47	77.51	77.47	73.28	76.78
	MPLMM	65.93	77.10	65.28	74.02	79.75	78.74	77.45	77.84	77.97	77.95	77.97	77.95	74.06	77.27
	REP	67.19	78.22	66.62	75.81	81.09	80.08	78.57	79.29	79.31	79.29	79.31	79.29	75.35	78.66
MOSEI	MMIN	67.11	68.67	68.17	69.74	78.67	78.71	79.94	79.96	79.32	79.29	79.32	79.29	75.42	75.94
	LNLN	66.94	68.74	68.11	69.79	78.21	78.30	79.41	79.47	79.63	79.71	79.63	79.71	75.32	75.95
	MPLMM	67.33	68.71	68.21	69.91	79.12	79.17	80.45	80.43	80.11	80.13	80.11	80.13	75.89	76.41
	REP	68.58	70.05	69.98	71.25	80.46	80.51	81.68	81.77	81.33	81.47	81.33	81.47	77.23	77.75
MOSI	MMIN	59.16	60.12	61.01	61.98	80.10	80.16	63.79	64.08	80.50	80.33	80.46	80.63	70.84	71.22
	LNLN	62.26	62.35	61.63	62.12	79.81	80.10	64.54	64.33	79.89	79.84	80.74	80.93	70.48	70.11
	MPLMM	62.71	63.65	63.12	63.74	80.12	80.31	65.02	65.41	80.76	81.09	81.12	81.19	72.14	72.57
	REP	64.25	65.28	64.86	65.41	81.43	81.52	66.38	66.79	81.72	81.83	81.72	81.83	73.73	73.78

REP exhibits consistent benefits across various missing-modality patterns and datasets, validating the effectiveness of its feature buffering and replay strategy in mitigating information degradation and enhancing robustness under modality-incomplete conditions.

4.3 Results on VLA tasks

We adopt a pre-training and prompt-tuning pipeline using a frozen Mult backbone [33], trained with random modality missing to enhance robustness. Experiments are conducted on CH-SIMS, MOSEI, and MOSI, and compared with MMIN [36], LNLN [23], and MPLMM [11]. As shown in Table 2, REP consistently achieves the best performance across all single-modality missing scenarios.

REP performs strongly in dual-modality missing settings such as Audio-only and Image-only. When text is the only remaining modality, REP achieves the highest accuracy on all benchmarks, reaching 81.09% on CH-SIMS and 80.46% on MOSEI. Across all missing-modality conditions, REP delivers the best overall results on the three datasets, with F1 scores of 78.66 on CH-SIMS and 77.75 on MOSEI. These findings show that the cross-layer replay mechanism provides effective compensation for missing and enables performance in multimodal sentiment recognition.

4.4 Results on AS task

The MOD dataset consists of acoustic (8kHz) and seismic (100Hz) signals collected for vehicle and pedestrian classification, covering a total of seven classes. We evaluate the proposed REP method on this dataset, focusing on its performance on time-series sensor modalities. The comparison methods include Swin Transformer (Baseline) and FOCAL, and the results are shown in the figure below:

Experimental results show that different vehicles produce significantly different ground vibration patterns, and the absence of this modality leads to a substantial drop in accuracy, especially when the missing rate exceeds 50%. Methods without prompt-based adaptation suffer from a larger performance decline in such scenarios. Our proposed REP effectively mitigates the performance degradation caused by missing time-series sensor signals through feature replay and information compensation, demonstrating stronger robustness across all missing rates as well as the potential to be extended to more modalities.

4.5 Ablation study

In this section, we will conduct ablation studies to investigate the following aspects: (1) the impact of noise ratios/types in initialization, (2) the impact of the replay mechanism, (3) the impact of private-shared feature separation, and (4) how buffer configurations influence computational cost, parameters, and overall performance.

Module ablation. To evaluate the effectiveness of each component, we conduct ablation experiments on the Food101 dataset under a missing-modality rate of $\eta = 70\%$. As shown in Table 3, we progressively add dynamic initialization,

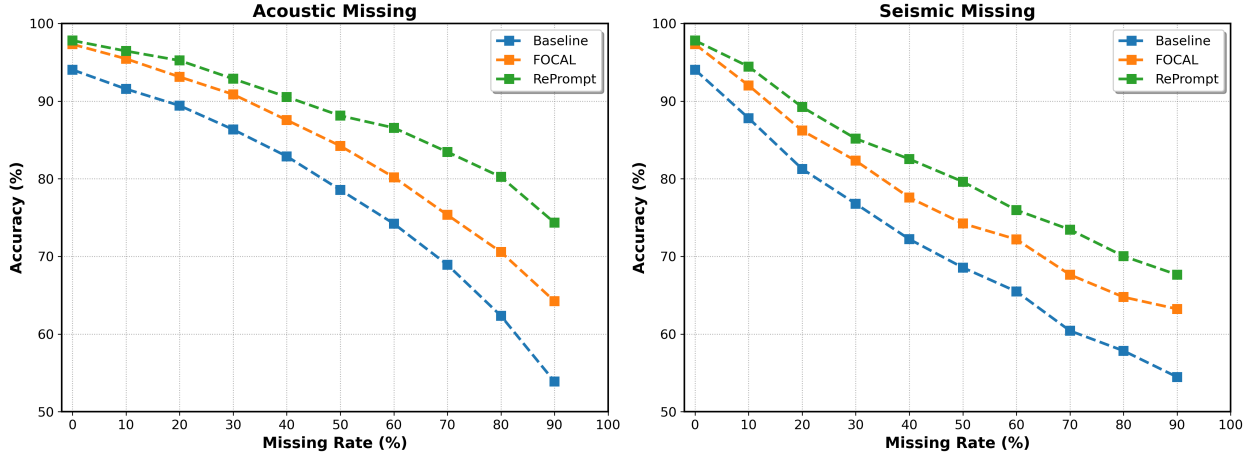


Figure 4: Modal missing tests on acoustic-seismic temporal sensor modalities.

private-shared feature separation, and the replay mechanism on top of the CLIP baseline to examine their individual contributions. Furthermore, in Table 4, we investigate the additional effects of removing the private or shared buffer, as well as the impact of different noise types used during initialization.

Table 3: Ablation study on main components of REP($\eta = 70\%$).

Method Variant	Text-missing	Image-missing	Both-missing
Baseline	70.42	78.00	73.02
+ Dynamic Initialization	73.11	80.42	75.48
+ Dual buffers	76.84	83.91	78.91
+ Replay (Full REP)	80.40	87.32	82.68

Table 4: Ablation of buffers and noise types ($\eta = 70\%$).

Method Variant	Text-missing	Image-missing	Both-missing
Full REP	80.40	87.22	82.68
w/o Private Buffer	78.74	85.92	81.05
Gaussian \rightarrow Uniform	79.11	85.36	81.08
Gaussian \rightarrow Laplace	78.85	85.92	81.14

The results in Table 3 show that each module in REP contributes steadily to performance improvements. Dynamic initialization provides a clear initial gain, while introducing dual private-shared buffers further enhances robustness under all missing-modality conditions. Adding the replay mechanism yields the largest improvement, highlighting its role in recovering early-layer information and stabilizing predictions when inputs are incomplete.

Table 4 further examines the design choices within REP. Removing either the private buffer leads to consistent performance drops, indicating that decoupling is necessary. Finally, replacing Gaussian noise in initialization with uniform or Laplace noise results in slightly lower accuracy, confirming that the proposed initialization strategy is effective and well aligned with the learning dynamics of REP.

In addition, we investigate the influence of the noise ratio ϵ_n . As shown in the Figure 6, although $\epsilon_n = 0.3$ yields the best performance in image-missing, the overall average performance is highest when $\epsilon_n = 0.2$. Therefore, we adopt $\epsilon_n = 0.2$ as the default setting for all experiments.

Buffer settings and Efficiency analysis. Large buffer sizes inevitably increase both computational overhead and parameter count, while offering limited additional performance benefits. To better understand this trade-off, we systematically vary the prompt length and buffer depth. As shown in Figure 5, the model achieves the best performance when the depth is set to 6 and the prompt length to 36, beyond which the gains saturate or even slightly decline.

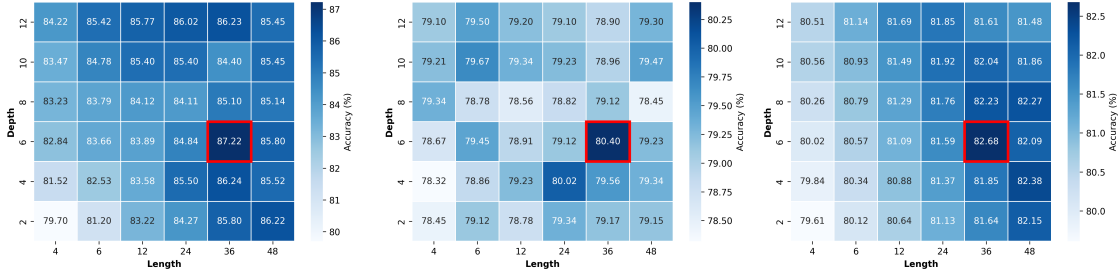


Figure 5: Ablation study on REP buffer configuration. Results are under 70% missing rate. From left to right are the text-missing, image-missing, and both-missing settings, respectively.

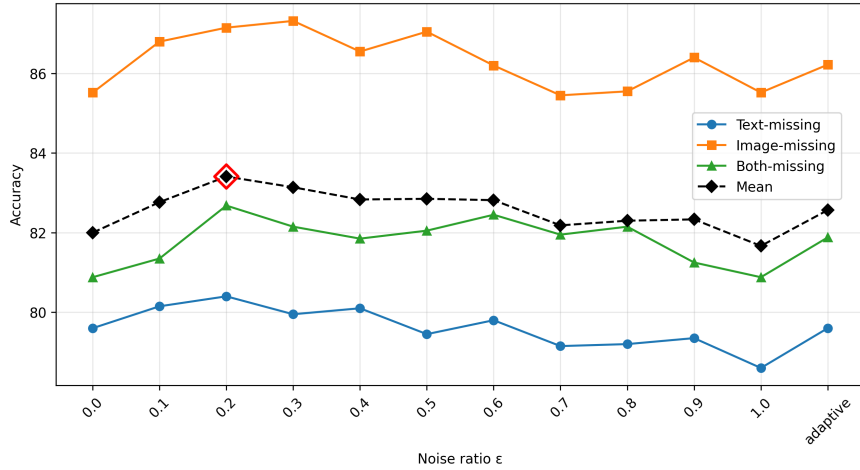


Figure 6: Ablation study on the value of noise factor ϵ_{τ} .

To further ensure fairness when comparing with existing methods, we additionally control the number of learnable parameters by adjusting the prompt length. The results are summarized in Table 5.

Table 5: Efficiency analysis of REP on Food-101

Method	Params (M)					
	0.08	0.64	1.12	1.6	2.08	2.56
MAP	77.52	78.14	78.59	79.08	79.24	79.11
DCP	80.04	80.89	80.82	81.87	81.80	81.76
Ours	81.16	82.04	82.23	82.68	81.85	81.64

Under the same parameters incrementation, REP consistently outperforms MAP and DCP. Moreover, it achieves strong robustness in missing-modality scenarios without requiring a large increase in parameters. These findings indicate that REP provides a favorable balance between efficiency and performance.

5 Conclusion

REP is designed to address the core challenge of information decay in missing-modality scenarios. By introducing dynamic initialization, private-shared feature decomposition, and cross-layer replay, REP effectively preserves early-layer representations and compensates for incomplete inputs. The experimental results across VL and VLA benchmarks confirm that REP successfully mitigates the limitations outlined in our motivation and delivers consistent robustness improvements.

References

- [1] Alec Radford, Jong Wook Kim, Chris Hallacy, Aditya Ramesh, Gabriel Goh, Sandhini Agarwal, Girish Sastry, Amanda Askell, Pamela Mishkin, Jack Clark, et al. Learning transferable visual models from natural language supervision. In *International conference on machine learning*, pages 8748–8763. PMLR, 2021.
- [2] Andrey Guzhov, Federico Raue, Jörn Hees, and Andreas Dengel. Audioclip: Extending clip to image, text and audio. In *ICASSP 2022-2022 IEEE International Conference on Acoustics, Speech and Signal Processing (ICASSP)*, pages 976–980. IEEE, 2022.
- [3] Zilong Wang, Zhaohong Wan, and Xiaojun Wan. Transmodality: An end2end fusion method with transformer for multimodal sentiment analysis. In *Proceedings of the web conference 2020*, pages 2514–2520, 2020.
- [4] Guimin Hu, Ting-En Lin, Yi Zhao, Guangming Lu, Yuchuan Wu, and Yongbin Li. Unimse: Towards unified multimodal sentiment analysis and emotion recognition. In *Proceedings of the 2022 Conference on Empirical Methods in Natural Language Processing*, pages 7837–7851. Association for Computational Linguistics, 2022.
- [5] Antoine Yang, Arsha Nagrani, Paul Hongsuck Seo, Antoine Miech, Jordi Pont-Tuset, Ivan Laptev, Josef Sivic, and Cordelia Schmid. Vid2seq: Large-scale pretraining of a visual language model for dense video captioning. In *Proceedings of the IEEE/CVF Conference on Computer Vision and Pattern Recognition*, pages 10714–10726, 2023.
- [6] Haotian Liu, Chunyuan Li, Qingyang Wu, and Yong Jae Lee. Visual instruction tuning. *Advances in neural information processing systems*, 36, 2024.
- [7] Shilong Liu, Zhaoyang Zeng, Tianhe Ren, Feng Li, Hao Zhang, Jie Yang, Qing Jiang, Chunyuan Li, Jianwei Yang, Hang Su, et al. Grounding dino: Marrying dino with grounded pre-training for open-set object detection. In *European Conference on Computer Vision*, pages 38–55. Springer, 2025.
- [8] Mengmeng Ma, Jian Ren, Long Zhao, Sergey Tulyakov, Cathy Wu, and Xi Peng. Smil: Multimodal learning with severely missing modality. In *Proceedings of the AAAI Conference on Artificial Intelligence*, volume 35, pages 2302–2310, 2021.
- [9] Jaehyuk Jang, Yooseung Wang, and Changick Kim. Towards robust multimodal prompting with missing modalities. In *ICASSP 2024-2024 IEEE International Conference on Acoustics, Speech and Signal Processing (ICASSP)*, pages 8070–8074. IEEE, 2024.
- [10] Hu Wang, Yuanhong Chen, Congbo Ma, Jodie Avery, Louise Hull, and Gustavo Carneiro. Multi-modal learning with missing modality via shared-specific feature modelling. In *Proceedings of the IEEE/CVF Conference on Computer Vision and Pattern Recognition*, pages 15878–15887, 2023.
- [11] Zirun Guo, Tao Jin, and Zhou Zhao. Multimodal prompt learning with missing modalities for sentiment analysis and emotion recognition. In *Proceedings of the 62nd Annual Meeting of the Association for Computational Linguistics (Volume 1: Long Papers)*, pages 1726–1736, 2024.
- [12] Yi-Lun Lee, Yi-Hsuan Tsai, Wei-Chen Chiu, and Chen-Yu Lee. Multimodal prompting with missing modalities for visual recognition. In *Proceedings of the IEEE/CVF Conference on Computer Vision and Pattern Recognition*, pages 14943–14952, 2023.
- [13] Lianyu Hu, Tongkai Shi, Wei Feng, Fanhua Shang, and Liang Wan. Deep correlated prompting for visual recognition with missing modalities. In *Advances in Neural Information Processing Systems (NeurIPS)*, 2024.
- [14] Menglin Jia, Luming Tang, Bor-Chun Chen, Claire Cardie, Serge Belongie, Bharath Hariharan, and Ser-Nam Lim. Visual prompt tuning. In *European Conference on Computer Vision*, pages 709–727. Springer, 2022.
- [15] Kaiyang Zhou, Jingkang Yang, Chen Change Loy, and Ziwei Liu. Learning to prompt for vision-language models. *International Journal of Computer Vision*, 130(9):2337–2348, 2022.
- [16] Kaiyang Zhou, Jingkang Yang, Chen Change Loy, and Ziwei Liu. Conditional prompt learning for vision-language models. In *Proceedings of the IEEE/CVF conference on computer vision and pattern recognition*, pages 16816–16825, 2022.
- [17] Anastasia Razdaibiedina, Yuning Mao, Rui Hou, Madian Khabza, Mike Lewis, and Amjad Almahairi. Progressive prompts: Continual learning for language models. In *The Eleventh International Conference on Learning Representations*, 2023.
- [18] Mengmeng Ma, Jian Ren, Long Zhao, Davide Testuggine, and Xi Peng. Are multimodal transformers robust to missing modality? In *Proceedings of the IEEE/CVF Conference on Computer Vision and Pattern Recognition*, pages 18177–18186, 2022.
- [19] Donggeun Kim and Taesup Kim. Missing modality prediction for unpaired multimodal learning via joint embedding of unimodal models. In *European Conference on Computer Vision*, pages 171–187. Springer, 2025.

- [20] Dongjun Lee, Seokwon Song, Jihee Suh, Joonmyeong Choi, Sanghyeok Lee, and Hyunwoo J Kim. Read-only prompt optimization for vision-language few-shot learning. In *Proceedings of the IEEE/CVF International Conference on Computer Vision*, pages 1401–1411, 2023.
- [21] Muhammad Uzair Khattak, Hanoona Rasheed, Muhammad Maaz, Salman Khan, and Fahad Shahbaz Khan. Maple: Multi-modal prompt learning. In *Proceedings of the IEEE/CVF Conference on Computer Vision and Pattern Recognition*, pages 19113–19122, 2023.
- [22] Ji Zhang, Shihan Wu, Lianli Gao, Heng Tao Shen, and Jingkuan Song. Dept: Decoupled prompt tuning. In *Proceedings of the IEEE/CVF Conference on Computer Vision and Pattern Recognition*, pages 12924–12933, 2024.
- [23] Haoyu Zhang, Wenbin Wang, and Tianshu Yu. Towards robust multimodal sentiment analysis with incomplete data. *Advances in Neural Information Processing Systems*, 37:55943–55974, 2024.
- [24] Huilin Chen, Miaomiao Cai, Fan Liu, Zhiyong Cheng, Richang Hong, and Meng Wang. I3-mrec: Invariant learning with information bottleneck for incomplete modality recommendation. In *Proceedings of the 33rd ACM International Conference on Multimedia*, pages 6133–6142, 2025.
- [25] Ziyi Li, Wei-Long Zheng, and Bao-Liang Lu. Multimodal emotion recognition with missing modality via a unified multi-task pre-training framework. In *Proceedings of the 33rd ACM International Conference on Multimedia*, pages 5717–5725, 2025.
- [26] Rui Liu, Haolin Zuo, Zheng Lian, Hongyu Yuan, and Qi Fan. Hardness-aware dynamic curriculum learning for robust multimodal emotion recognition with missing modalities. In *Proceedings of the 33rd ACM International Conference on Multimedia*, pages 5755–5764, 2025.
- [27] Donggeun Kim and Taesup Kim. Missing modality prediction for unpaired multimodal learning via joint embedding of unimodal models. In *European Conference on Computer Vision*, pages 171–187. Springer, 2024.
- [28] John Arevalo, Tamar Solorio, Manuel Montes-y Gómez, and Fabio A González. Gated multimodal units for information fusion. *arXiv preprint arXiv:1702.01992*, 2017.
- [29] Lukas Bossard, Matthieu Guillaumin, and Luc Van Gool. Food-101 – mining discriminative components with random forests. In *European Conference on Computer Vision*, 2014.
- [30] Douwe Kiela, Hamed Firooz, Aravind Mohan, Vedanuj Goswami, Amanpreet Singh, Pratik Ringshia, and Davide Testuggine. The hateful memes challenge: Detecting hate speech in multimodal memes. *Advances in neural information processing systems*, 33:2611–2624, 2020.
- [31] Wenmeng Yu, Hua Xu, Fanyang Meng, Yilin Zhu, Yixiao Ma, Jiele Wu, Jiyun Zou, and Kaicheng Yang. Ch-sims: A chinese multimodal sentiment analysis dataset with fine-grained annotation of modality. In *Proceedings of the 58th annual meeting of the association for computational linguistics*, pages 3718–3727, 2020.
- [32] Amir Zadeh, Rowan Zellers, Eli Pincus, and Louis-Philippe Morency. Mosi: multimodal corpus of sentiment intensity and subjectivity analysis in online opinion videos. *arXiv preprint arXiv:1606.06259*, 2016.
- [33] Yao-Hung Hubert Tsai, Shaojie Bai, Paul Pu Liang, J. Zico Kolter, Louis-Philippe Morency, and Ruslan Salakhutdinov. Multimodal transformer for unaligned multimodal language sequences. In *Proceedings of the 57th Annual Meeting of the Association for Computational Linguistics (Volume 1: Long Papers)*, Florence, Italy, 7 2019. Association for Computational Linguistics.
- [34] AmirAli Bagher Zadeh, Paul Pu Liang, Soujanya Poria, Erik Cambria, and Louis-Philippe Morency. Multimodal language analysis in the wild: Cmu-mosei dataset and interpretable dynamic fusion graph. In *Proceedings of the 56th Annual Meeting of the Association for Computational Linguistics (Volume 1: Long Papers)*, pages 2236–2246, 2018.
- [35] Shengzhong Liu, Tomoyoshi Kimura, Dongxin Liu, Ruijie Wang, Jinyang Li, Suhas Diggavi, Mani Srivastava, and Tarek Abdelzaher. Focal: Contrastive learning for multimodal time-series sensing signals in factorized orthogonal latent space. *Advances in Neural Information Processing Systems*, 36:47309–47338, 2023.
- [36] Jinming Zhao, Ruichen Li, and Qin Jin. Missing modality imagination network for emotion recognition with uncertain missing modalities. In *Proceedings of the 59th Annual Meeting of the Association for Computational Linguistics and the 11th International Joint Conference on Natural Language Processing (Volume 1: Long Papers)*, pages 2608–2618, 2021.

6 Appendix

6.1 More Results

This section presents additional results of REP on vision-language (VL) tasks. We conduct evaluations on three multi-modal benchmark datasets—Food-101, MMIMDB, and Hateful Memes—to verify REP’s robustness and generalization under various modality-missing scenarios.

Complete Training Setup. All models are trained on fully available image-text pairs. At test time, we gradually increase the missing rate η from 0%, 30%, 50%, 70% to 90% to simulate different levels of information loss. We use the pre-trained CLIP as the baseline, and compare REP against state-of-the-art methods including MAP, MMP, and DCP.

As shown in Figure 7, under no missing conditions, all methods perform comparably (CLIP baseline: 90.06). However, as the missing rate increases, REP exhibits significantly slower performance degradation. For example, under 30% text missing, REP achieves an accuracy of 86.05, outperforming DCP (85.20), MAP (83.94), and CLIP (82.93) by 1.8%–3.12%. Even under 50% image missing, REP still maintains 88.56 accuracy, almost equal to the no-missing baseline.

In extreme missing scenarios ($\eta \geq 70\%$), REP shows even more pronounced advantages. For example, with 70% missing, REP achieves 83.01 accuracy, surpassing MAP (75.66) and CLIP (76.69) by 7.35% and 6.32%, respectively. Even with 100% modality missing, REP still achieves 72.05 (image-only) and 78.91 (text-only), significantly outperforming all baselines.

These results confirm that REP, trained on complete data, effectively captures both single-modality and cross-modality signals, enabling strong robustness under modality-missing conditions. It prevents the performance collapse commonly observed in traditional models relying solely on a single modality.

Cross-Dataset Generalization. To further verify REP’s robustness in broader settings, we evaluate it on MMIMDB and Hateful Memes, two widely used multimodal benchmarks.

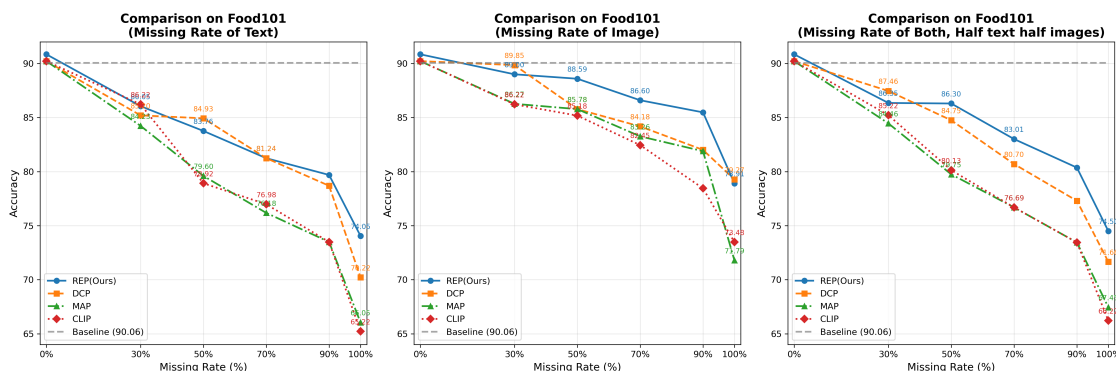


Figure 7: Evaluation on the Food-101 dataset under full training setup. All models are trained with 100% image and text data. The three subplots show results under text-missing, image-missing, and both-modality-missing settings, respectively.

As shown in Figure 8 and 9, REP consistently outperforms prior methods across both datasets, especially under severe or single-modality-missing conditions.

On MMIMDB, REP achieves 58.29 F1-Macro with no missing, slightly outperforming the baseline (57.76). With 30% text missing, REP achieves 56.05, outperforming DCP (55.20), MMP (54.94), and the baseline (52.93). Even under 100% text missing, REP maintains 49.02 F1-Macro, outperforming others by 2.77%–4.11%.

On Hateful Memes, REP achieves 68.48 AUROC with 30% image missing, outperforming DCP (67.56) and baseline (65.35). Under 100% image missing, REP still reaches 59.13 AUROC, surpassing the baseline (55.28) by 3.85% and outperforming MMP (57.92) and DCP (58.86).

When both modalities are heavily missing (e.g., 90% each), REP continues to lead with 65.11 AUROC, outperforming DCP (64.62) and MMP (63.94). In text-only and image-only testing scenarios, REP still shows clear advantages. For instance, on Hateful Memes, REP achieves 61.22 (text-only) and 59.13 (image-only) AUROC, outperforming the baseline (56.21 and 55.28).

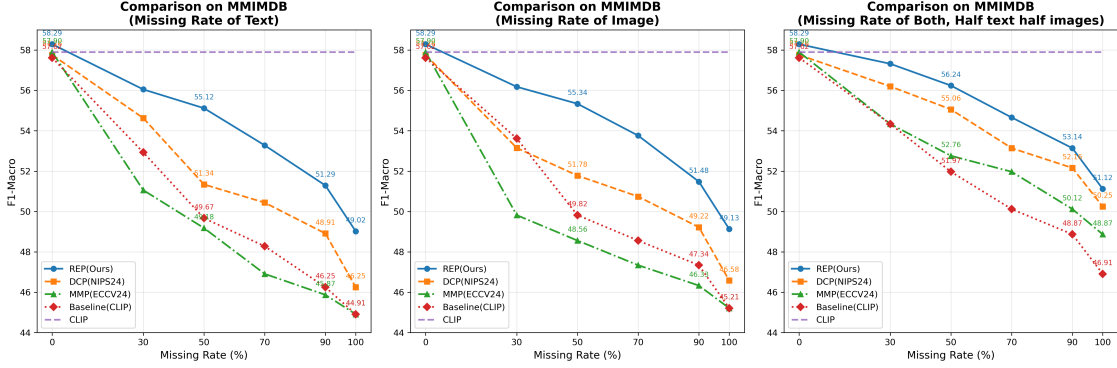


Figure 8: Evaluation on MMIMDB under full training. All models are trained with complete data and evaluated under varying missing rates.

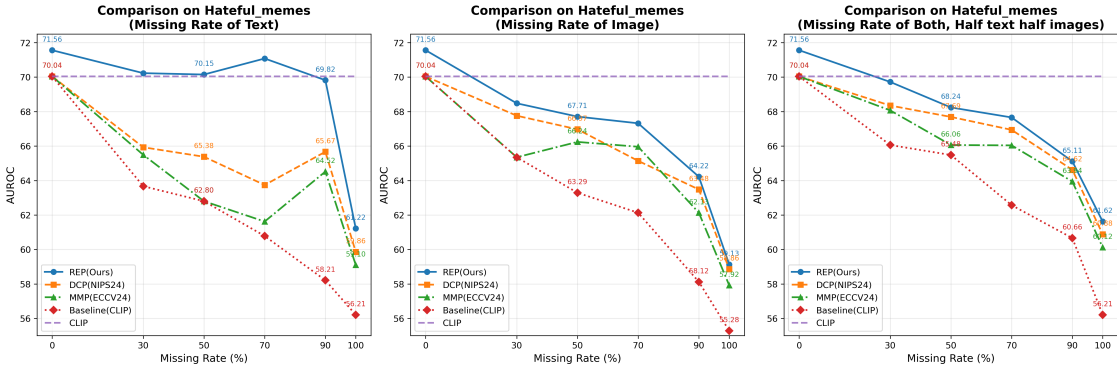


Figure 9: Evaluation on Hateful Memes under full training. All models are trained with complete data and evaluated under varying missing rates.

Furthermore, REP demonstrates significantly slower performance degradation compared to baselines. On MMIMDB, increasing the text missing rate from 0% to 100% results in only a 9.27-point drop in REP’s F1-Macro (from 58.29 to 49.02), while the baseline drops by 12.85 points. Similarly, on Hateful Memes, REP’s AUROC decreases by 12.43 (from 71.56 to 59.13), while the baseline drops by 14.76.

6.2 More Ablation on Buffer

We conduct ablation studies to analyze how the buffer length L and depth D affect model performance. Experiments are performed on MMIMDB and Hateful Memes under 70% missing rate, covering three scenarios: text missing, image missing, and both-missing. Figure 9 reports the results.

The optimal performance is generally achieved when $L = 36$ and $D = 6$. In MMIMDB’s text-missing setting, REP achieves 53.71 at $L = 36, D = 6$, clearly higher than nearby configurations (e.g., 52.68 at $L = 24$). Similarly, for Hateful Memes in the full-modality setting, performance peaks at 66.89 with $L = 36$, but drops to 66.24 when $L = 48$. As L or D increases further, the performance shows diminishing returns or even degradation, likely due to feature redundancy or computation overhead. For instance, increasing D from 6 to 12 at $L = 36$ on Hateful Memes degrades performance from 66.89 to 66.05. This suggests that overly deep or long buffers may harm aggregation.

6.3 Comparison with Multimodal Large Models

We compare REP with open-source multimodal LLMs: LLaVA-v1.5-7B and Qwen2-VL-7B-Instruct, under missing-modality settings on Hateful Memes. Results are shown in Table 6.

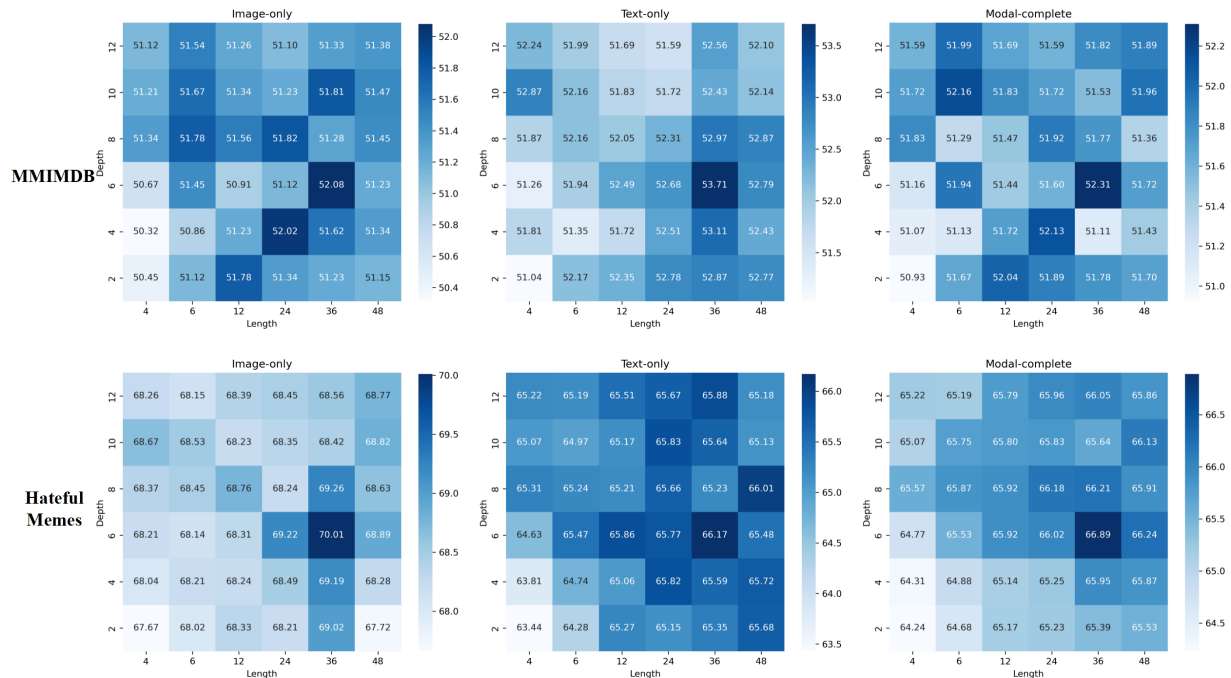


Figure 10: Ablation on buffer length and depth. Top: MMIMDB. Bottom: Hateful Memes. Each column corresponds to a different missing setting.

Table 6: Performance comparison on Hateful Memes with different modality-missing conditions.

Method	Image	Text	Accuracy	AUROC
DCP	100%	30%	69.89	64.12
	30%	100%	67.85	65.48
	65%	65%	68.92	66.08
REP	100%	30%	71.25	70.01
	30%	100%	68.22	66.17
	65%	65%	70.41	66.89
LLaVA-7B	100%	30%	55.44	50.32
	30%	100%	63.57	57.25
	65%	65%	60.48	58.12
Qwen2-7B	100%	30%	60.57	55.92
	30%	100%	65.98	62.44
	65%	65%	62.72	60.25

REP significantly outperforms both LLMs in all cases. Notably, under text-missing conditions, LLaVA and Qwen2 drop to near-random performance (AUROC 50.32 and 55.92), while REP maintains 70.01 AUROC. Considering the huge tuning cost of MLLMs, REP offers a lightweight and robust alternative.